Optical Materials 33 (2011) 1943–1947

Contents lists available at ScienceDirect

Optical Materials

journal homepage: www.elsevier.com/locate/optmat

Preparation of novel transparent glass–ceramics containing fluoride crystals

Takenobu Suzuki *, Shin-ichiro Masaki, Kento Mizuno, Yasutake Ohishi

Research Center for Advanced Photon Technology, Toyota Technological Institute, 2-12-1, Hisakata, Tempaku-Ku, Nagoya 468-8511, Japan

ARTICLE INFO

Article history:
Received 19 October 2010
Received in revised form 16 March 2011
Accepted 16 March 2011
Available online 8 April 2011

Keywords:
Transparent glass–ceramics
$YLiF_4$
Crystallization mechanism

ABSTRACT

Transparent glass–ceramics containing $YLiF_4$ nano-crystals were synthesized by controlled heat-treatments of $LiF—YF_3—Al_2O_3—SiO_2$ glass. The crystallite size estimated to be about 8 nm was much less than the wavelength of the visible light. The transmittance of the glass–ceramic with a thickness of 2 mm was more than 85% at 400 nm and as high as 95% in the infrared region. The fluorescence centered around 1000 nm was hardly observed from Er^{3+}-doped precursor glass under 800 nm excitation, while the emission with the Stark spitting was clearly observed for the Er^{3+}-doped glass–ceramic. The phonon sideband of the $^7F_0 \rightarrow {}^5D_2$ excitation spectra of Eu^{3+} reveals that Eu^{3+} doped in precursor glass is in silicate network while Eu^{3+} doped in the glass–ceramic is in not only silicate framework but also fluoride framework. These results indicate that rare-earth ions such as Er^{3+} and Eu^{3+} could be successfully incorporated into $YLiF_4$ nano-crystals in the glass–ceramics.

1. Introduction

In recent years, oxyfluoride glass–ceramics (GCs) have been attracting much attention because they have the high chemical and mechanical strength of oxide glass and the low effective phonon energy of fluoride crystal. The low phonon energy of fluoride crystal would enable emission from rare-earth energy levels that would be quenched in high phonon energy glasses. A GC containing crystals with a diameter of less than a few 10s of nano-meters is transparent even though there is a mismatch of the refractive indices of the glassy phase and crystalline phase. This is because the lightwave propagating in it can not feel a modulation of the refractive index in dimensions far shorter than its wavelength.

A rare-earth ion-doped transparent GC containing $Pb_xCd_{1-x}F_2$ nano-crystal was developed in 1993 [1]. The efficient optical amplification and lasing of Nd^{3+}-doped transparent GC containing PbF_2:CdF_2:YF_3 nano-crystal have been demonstrated [2]. These crystals are not necessarily good host materials for doping of rare earth ions because of the large differences in ionic radii and valence between the host and doped rare-earth ions. Moreover, Pb and Cd have been designated as specified toxic substances by the restriction hazardous substance (RoHS). Thus extensive studies have been done to explorer transparent oxyfluoride glass ceramics containing other crystals such as CaF_2 [3–7], LaF_3 [8–10], YF_3 [11–13] and so forth.

$YLiF_4$ has good optical properties such as high transparency throughout the ultraviolet (UV) to mid-infrared (IR), high UV damage resistance, low non-radiative decay rate, low optical lensing and low two absorption coefficient [14]. These properties make $YLiF_4$ one of the most popular rare-earth-doped laser materials, with the largest number of laser lines from the UV to mid-IR range among fluoride crystals [15]. Recently, Deng et al. prepared GCs containing $YLiF_4$ crystals [16,17]. Although the transparency of GCs crystals is one of the most important factors for optically active media, the transparency of their GCs containing $YLiF_4$ was not mentioned in detail in their reports. We have prepared a GC containing $YLiF_4$ nano-crystals with high transparency over the visible to IR region. Moreover, we have confirmed from the phonon sideband of Eu^{3+} emission and 1000 nm emission of Er^{3+} that Eu^{3+} and Er^{3+} doped in the GC exists partly in $YLiF_4$ nano-crystals. This indicates that rare-earth ions are successfully incorporated into $YLiF_4$ nano-crystals in the GC.

2. Experimental

Glasses in 20 g batches were prepared using reagent grade LiF, YF_3, Al_2O_3 and SiO_2 powders. The glass composition was $27LiF—17YF_3—23Al_2O_3— 43SiO_2$ in mol.%. The GC was obtained by a conventional melt quenching of glass, followed by heat-treatment of the glass [3–13]. The mixed raw materials were melted in a Pt-Rh crucible at 1450 °C for 1 h in an electric furnace, in which oxygen gas was flowing during glass melting. After quenching on a steel plate preheated to 450 °C, the obtained glass was annealed at 450 °C for 1 h and then cooled slowly to room temperature in an electric furnace. The thermal properties were studied by a differential scanning calorimeter (Rigaku, ThermoPlus DSC 8270). About 40 mg of powdered glass was heated in a platinum pan at rates of 1–20 K/min in a temperature range of 30–1000 °C. The glass

* Corresponding author. Tel.: +81 52 809 1868.
E-mail address: takenobu@toyota-ti.ac.jp (T. Suzuki).

0925-3467/$ - see front matter © 2011 Elsevier B.V. All rights reserved.
doi:10.1016/j.optmat.2011.03.035

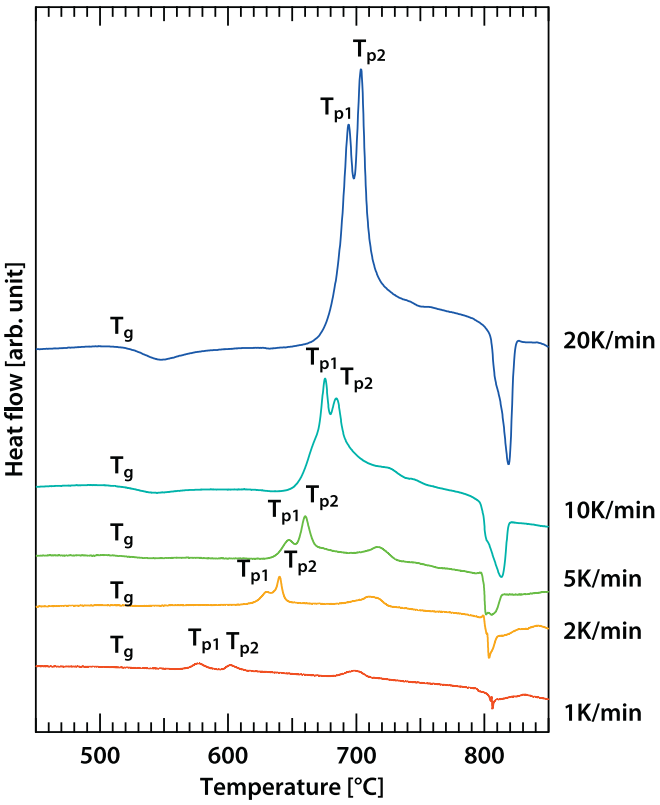

Fig. 1. Differential scanning calorimetry curves of the precursor glass.

transition temperature (T_g) was determined from the tangent intersections of the endothermic peak in the differential scanning calorimetry (DSC) curve. The crystallization temperature (T_p) was obtained from the peak temperature of the exothermic peak. Heat-treatment was performed in an electric furnace in air in order to obtain GC from the precursor glass (PG). The PG was heated to heat-treatment temperatures of 530–600 °C at a rate of 10 K/min. The temperature was maintained within ±2 K for 2 h and then the heat-treated sample was cooled slowly to room temperature in the electric furnace.

Powder X-ray diffraction (XRD) measurements were carried out using a diffractometer (Shimadzu, XRD-6100) with the monochromatic Cu$K\alpha_1$ line (0.1540562 nm) and a 2θ range of 10–80 ° to identify crystalline phases precipitated in glass matrices. The average diameter (d) of crystallites in glass–ceramic samples was estimate from the full width at half maximum of the strongest diffraction peak by the Scherrer's equation [19,18]. The instrumental contribution for the width of the peak was checked using silicon powders with a diameter of ~44 μm.

As-quenched and heat-treated samples were cut to a thickness of 2 mm and polished to optical quality before subjecting them to optical measurements. UV-visible-near-IR absorption spectra were recorded in the wavelength range of 250–3300 nm using a double-beam spectrophotometer (Perkin-Elmer, Lambda900). The refractive indices were measured by a prism coupler (Metricon, 2010) at the wavelengths of 632.8, 974, 1320 and 1544 nm. Near-IR fluorescence spectra from the Er^{3+}-doped samples were measured by using a 800 nm laser diode as an excitation source and an InGaAs photo-diode (Hamamatsu Photonics, G5852-11) as a detector, in order to clarify the coordination states of Er^{3+} ions doped in the samples. Visible fluorescence spectra from the Eu^{3+}-doped samples

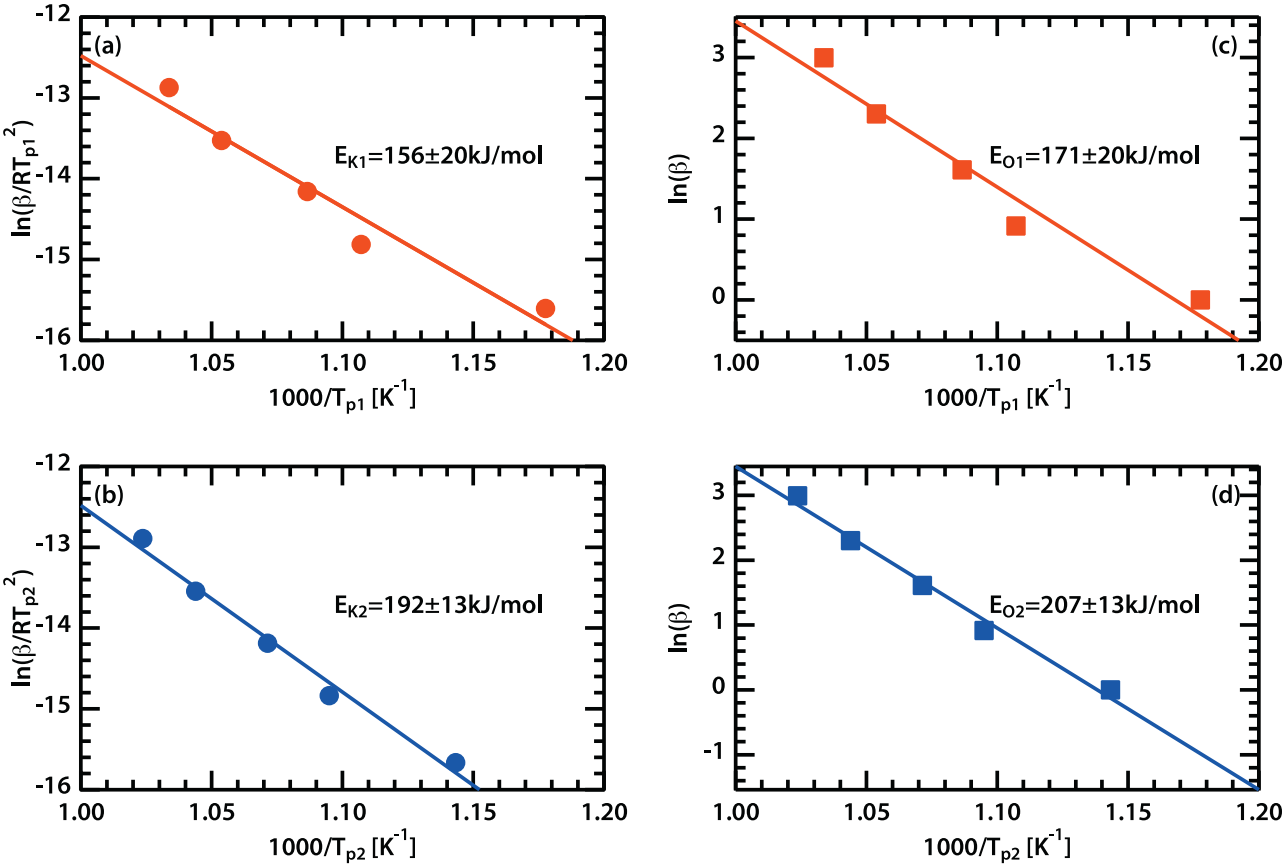

Fig. 2. Kissinger plots of (a) the first crystallization and (b) the second crystallization and Ozawa plots of (c) the first crystallization and (d) the second crystallization.

were measured by using a fluorescence spectrometer (Perkin-Elmer, LS55) at room temperature. The phonon sidebands in excitation spectra of the $^7F_0 \rightarrow {}^5D_2$ transition of Eu^{3+} were observed in order to clarify the coordination states of Eu^{3+} ions doped in the samples.

3. Results and discussions

Fig. 1 shows the DSC curves of powdered PG at heating rates of 1–20 K/min. An endothermic peak (T_g) around 520 °C can be attributed to the glass transition. The first exothermic peaks (T_{p1}) could be attributed, by XRD analysis as shown later, to the crystallization of $YLiF_4$ phase. The second exothermic peaks (T_{p2}) could be attributed to the crystallization of AlF_3 phase. The crystallization peaks shifted to higher temperatures with increasing heating rate. In order to investigate the crystallization kinetics, the apparent activation energies of crystallization were obtained using the Kissinger's equation and Ozawa's equation [20] as follows:

$$\frac{d\left[\ln\left(\beta/T_p^2\right)\right]}{d(1/T_p)} = -\frac{E}{R} \quad (1)$$

$$\frac{d\ln\beta}{d(1/T_p)} = -\frac{E}{R} \quad (2)$$

where β is heating rate, T_p is peak crystallization temperature, E is activation energy of crystallization. Fig. 2 shows Kissinger and Ozawa plots of the first and second crystallization. The activation energies of the first (E_{K1}) and the second (E_{K2}) crystallization estimated by Kissinger's equation were about 156 ± 20 kJ/mol and 192 ± 13 kJ/mol, respectively. The activation energy obtained by Ozawa equation was close to that by Kissinger equation. The activation energies of estimated by Ozawa's equation were about E_{O1} = 171 ± 20 kJ/mol and E_{O2} = 207 ± 13 kJ/mol. These activation energies are less than the dissociation energy of Al—O (222–423 kJ/mol [21]), Y—F (298 kJ/mol [22])), Al—F (346 kJ/mol [22]), and Si—O (444 kJ/mol [21]) bonds, whose metal cations are classified as glass formers and intermediates in oxide and fluoride glasses. Thus it is thought that the glass framework would be unchanged during the first and second crystallizations.

Fig. 3 shows the XRD patterns of PG and glasses heat-treated at 530, 540, 545, 550, 570, 590 and 600 °C. PG exhibited two broad halos, characteristic of a glassy phase, in the XRD pattern. In contrast, sharp diffraction peaks due to crystalline phase was clearly observed in the XRD pattern of glasses heat-treated at the temperature of more than 545 °C. The diffraction peaks can be attributed to $YLiF_4$ (ICDD, #85-0806). The size of the $YLiF_4$ crystals in GC heat-treated at 550 °C was calculated using Scherrer's equation to be about 8 nm from the full width at the half maximum of the XRD peak at about $2\theta = 18°$. In the XRD pattern of 600 °C, the diffraction peaks due to AlF_3 could be found in addition to those due to $YLiF_4$. From these XRD patterns, we conclude that the first and the second exothermic peaks in the DSC curves correspond to the crystallization of $YLiF_4$ and AlF_3, respectively.

Fig. 4 shows the visible and near-IR internal transmission spectra of PG and GC heat-treated at 550 °C. The transmittance was corrected to eliminate the effects of reflection from the surfaces, using the measured refractive index. The refractive index at 632.8, 974, 1320 and 1544 nm was 1.564, 1.556, 1.552, and 1.550 for PG and slightly larger values of 1.569, 1.561, 1.557, and 1.555 for GC heat-treated at 550 °C. The transmittance was more than 85% at 400 nm and as high as 95% in the IR region for GC. Though a high transmittance was achieved, the transmittance was less than expected from the crystallite size from the XRD. The low transparency of the present GC in the UV region could be due to the aggregation of $YLiF_4$ nano-crystals.

Fig. 5 shows emission spectra around 1.0 μm of Er^{3+}-doped PG, GC heat-treated at 550 °C and $51ZrF_4$—$20BaF_4$—$4.5LaF_3$—$4.5AlF_3$—20NaF—0. $1ErF_3$ (in mol.%, ZBLAN) glass, by 800 nm excitation. Er^{3+} ions are excited to the $^4I_{9/2}$ level by 800 nm and then some of them relax to the $^4I_{11/2}$ level. The emission around 1000 nm corresponding to the radiative $^4I_{11/2} \rightarrow {}^4I_{15/2}$ transition of Er^{3+} was clearly observed for GC, though it was hardly observed for PG. This can be understood from the difference of the environments of Er^{3+} in the PG and GC. The total radiative transition rate of the $^4I_{11/2}$ level of Er^{3+} is known to be ≈100 s^{-1} [23]. The non-radiative relaxation processes of excited rare-earth ions are usually attributed to concentration quenching through energy migration between rare-earth ions, the presence of hydroxyl (—OH) group,

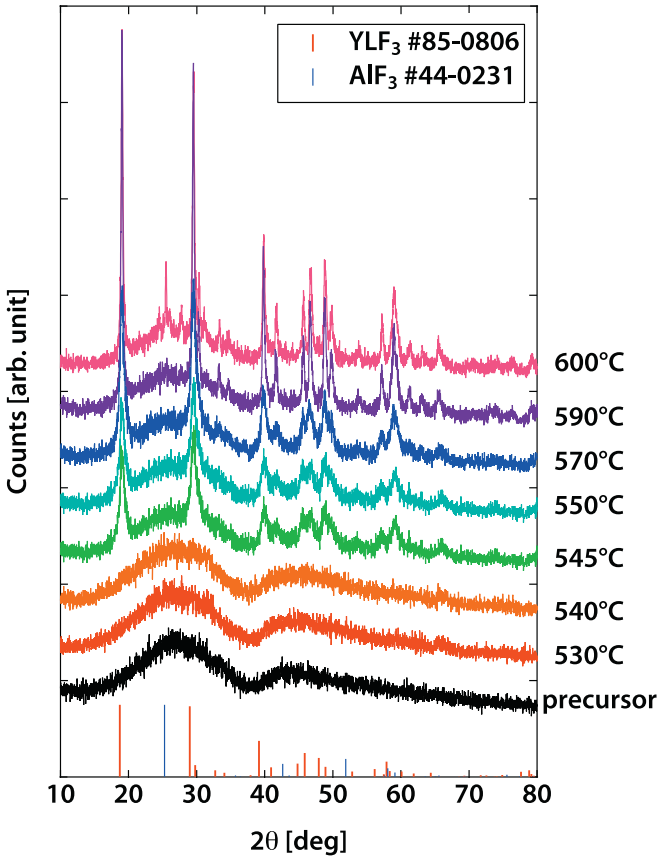

Fig. 3. X-ray diffraction powder patterns of precursor glass and glasses heat-treated at 530, 540, 545, 550, 570, 590 and 600 °C.

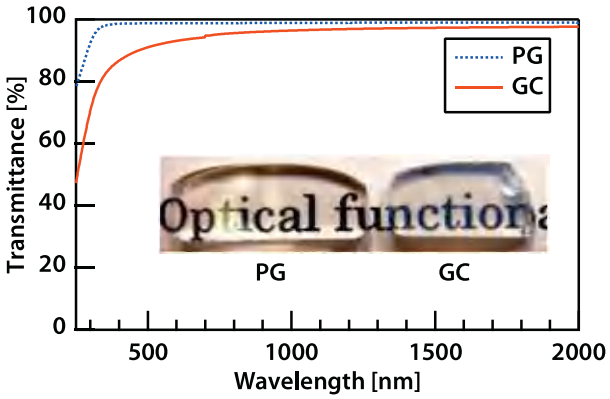

Fig. 4. Visible and near-infrared internal transmittance spectra of the precursor glass (PG) and glass–ceramic (GC) heat-treated at 550 °C. The inset figure shows a photograph of the PG and GC. The thickness of the samples is about 2. 0 mm.

and multi-phonon emission relaxation. We need not take into account concentration quenching effect in this case, since Er^{3+} concentration of PG and GC is same. —OH concentration estimated from the absorption coefficient at the peak of ~3000 cm^{-1} [24,25], was not changed by heat-treatment. Thus the rate of non-radiative transition by —OH group will not change by heat-treatment. The —OH concentration was as low as ~10^{18} cm^{-3} or ~30 ppm. The low —OH concentration is probably due to the addition of metal fluoride, which will liberate hydrogen species from the melt [26]. The non-radiative transition rate of the $^4I_{11/2} \rightarrow {}^4I_{13/2}$ transition by the multi-phonon emission relaxation in Er^{3+} depends largely on the highest phonon energy of the host material. The phonon energy of PG was about 1000 cm^{-1}, derived from a Raman spectrum measurement (not shown). This phonon energy is almost equal to the typical value in silicate glasses. The non-radiative transition rate of the $^4I_{11/2} \rightarrow {}^4I_{13/2}$ transition in the PG is estimated to be ≈10^4–10^5 s^{-1} for a phonon energy of 1000 cm^{-1} [27]. In this case, the emission from the $^4I_{11/2}$ level of Er^{3+} was hardly observed due to the instantaneous non-radiative transition by multi-phonon emission relaxation. In contrast, the typical non-radiative transition rate in fluorides is as low as ≈100 s^{-1}, because of the low phonon energy of fluorides (≈500–600 cm^{-1}) [15,27]. Since the radiative transition rate is comparable to the non-radiative transition rate in fluorides, the emission corresponding to the radiative $^4I_{11/2} \rightarrow {}^4I_{15/2}$ transition of Er^{3+} should be observed in fluorides. Therefore, the emission observed around 1000 nm from the Er-doped GC indicates that Er^{3+} ions doped in GC were incorporated into the fluoride phase. In addition, the Stark splitting could be resolved in the 1000 nm emission of the GC, though the emission from ZBLAN glass was featureless due to inhomogeneous broadening. This suggests that Er^{3+} ions doped in GC were successfully incorporated into $YLiF_4$ nano-crystals rather than a fluoride glassy phase.

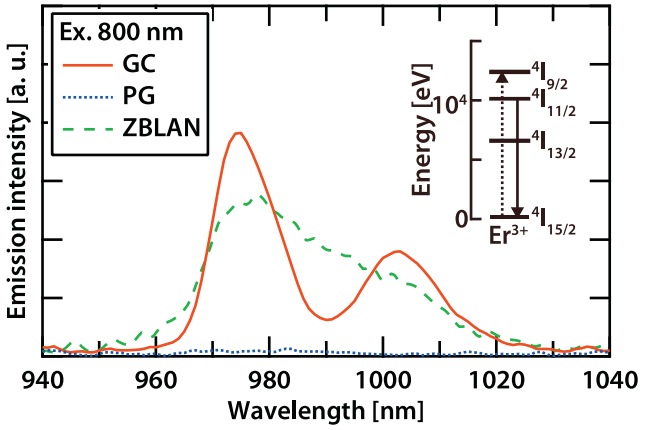

Fig. 5. Emission spectra of the $^4I_{11/2} \rightarrow {}^4I_{15/2}$ transition of the Er^{3+}-doped precursor glass (PG), glass–ceramic (GC) heat-treated at 550 °C and ZBLAN glass by 800 nm excitation. The inset figure is a simplified energy diagram of Er^{3+} ion.

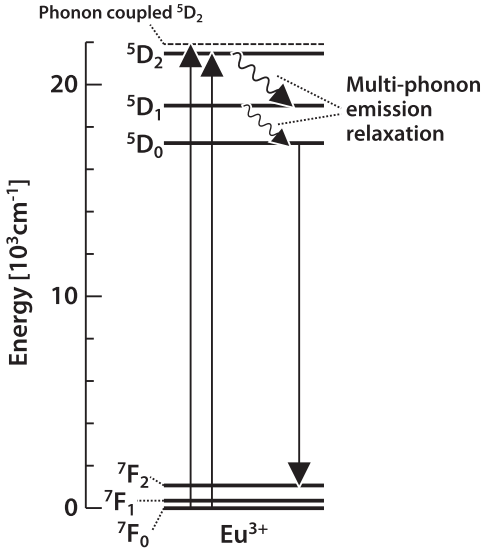

Fig. 6. Energy level diagram of Eu^{3+} coupled with phonon.

Fig. 6 shows energy level diagram of Eu^{3+} coupled with phonon. When an Eu^{3+} ion is excited to the phonon coupled or purely electronic $^5D_2$ state, the exited Eu^{3+} ion relaxes readily to the $^5D_0$ state involving multi-phonon emission. Then the Eu^{3+} ion relaxes to the $^7F_{0,1,2}$ states involving fluorescence. Thus the $^7F_0 \rightarrow {}^5D_2$ excitation spectrum of the $^5D_0 \rightarrow {}^7F_{0,1,2}$ emission gives the information of the phonon coupling of the $^5D_2$ state.

Fig. 7 shows the excitation spectra of Eu^{3+} doped in PG and GC heat-treated at 550 °C obtained by monitoring the $^5D_0 \rightarrow {}^7F_2$ emission at the peak of 615 nm. The inset figure shows the $^5D_0 \rightarrow {}^7F_{0,1,2}$ emission spectra excited at 465 nm of the $^7F_0 \rightarrow {}^5D_2$ transition. The maximum excitation peak corresponds to the zero-phonon line (ZPL) of the $^7F_0 \rightarrow {}^5D_2$ transition. The small peaks at higher photon energy correspond to phonon side bands (PSBs). PSB1 at about 940 cm^{-1} in Fig. 7 could be found for both PG and GC. PSB1 is due to silicate framework which normally gives the phonon energy of about 1000–1100 cm^{-1}. For the GC, PSB2 at about 640 cm^{-1} could be found in addition to PSB1. PSB2 is due to fluoride framework which normally gives the phonon energy of about 500–600 cm^{-1}. The area ratio of PSB2 to PSB1 of GC was about 0.08. Thus it is thought that about 8% of Eu^{3+} in GC exist in fluoride phase.

The thermal conductivity of glass–ceramic materials is an important property when they are to be employed as high power lasers and fiber amplifiers. Glass–ceramic materials have higher thermal conductivity values than glass but lower than crystals. For example, the thermal conductivity is about 1.4 W/m K for silica glass [28], 14 W/m K for $Y_3Al_5O_{12}$ garnet (YAG) crystal [29], and 5.4 for Li_2O—Al_2O_3—SiO_2 glass–ceramic [30]. Though the thermal conductivity of GC containing $YLiF_4$ nano-crystals is not known, it is expected to be in the range from 1.4 W/m K of silica glass to 6 W/m K of $YLiF_4$ crystal [29], which is higher than 0.63 W/m K of ZBLAN glass [28].

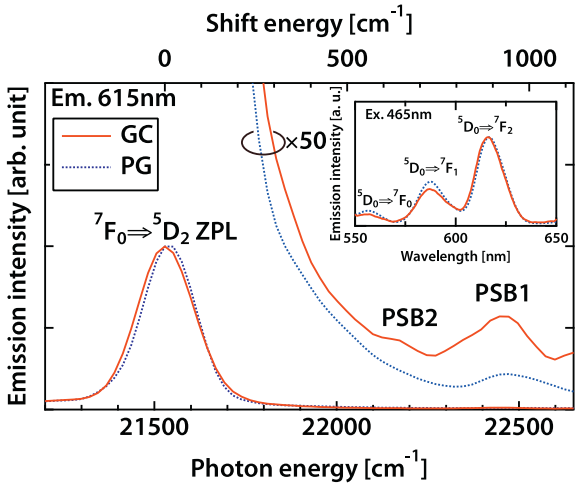

Fig. 7. Excitation spectra of Eu^{3+} doped in precursor glass (PG) and glass–ceramic (GC) heat-treated at 550 °C.

4. Summary

In summary, transparent glass–ceramics containing $YLiF_4$ nano-crystals were synthesized from conventionally melt-quenched $LiF—YF_3—Al_2O_3—SiO_2$ precursor glasses followed by controlled heat-treatment. The crystallite size was estimated to be about 8 nm, which is much less than the wavelength of the visible light. The internal transmittance of the glass–ceramic with a thickness of 2 mm was more than 85% at 400 nm and as high as 95% in the infrared region. The fluorescence centered around 1000 nm was hardly observed from Er^{3+}-doped precursor glass under 800 nm excitation, while the emission with the Stark spitting was clearly observed for the Er^{3+}-doped glass–ceramic. The phonon sideband of the $^7F_0 \rightarrow {}^5D_2$ excitation spectra of Eu^{3+} reveals that Eu^{3+} doped in precursor glass is in silicate network while Eu^{3+} doped in the glass–ceramic is in fluoride framework as well as in silicate framework. These results indicate that rare-earth ions such as Er^{3+} and Eu^{3+} could be successfully incorporated into $YLiF_4$ nano-crystals in the glass–ceramics.

The incorporation of rare-earth ions such as Er^{3+} and Eu^{3+} into $YLiF_4$ nano-crystals in a transparent glass–ceramic could open avenues to develop efficient laser media.

Acknowledgements

The authors should like to thank Dr. Shintaro Mizuno of Toyota Central R&D Labs. Inc. for his helpful discussion. This work was supported by the MEXT as a part of "Ultra-octave lightwave processing project" (2006–2010) of Private University High-tech Research Center.

References

[1] Y. Wang, . Ohwaki, Appl. Phys. Lett. 63 (1993) 3268.
[2] B.N. Samson, P.A. Tick, N.F. Borrelli, Opt. Lett. 26 (2001) 145.
[3] J. Fu, .M. Parker, P.S. Flower, R.M. Brown, Mater. Res. Bull. 37 (2002) 1843.
[4] X. Qiao, X. Fan, J. Wang, M. Wang, J. Non-cryst. Solids 351 (2005) 357.
[5] D. Chen, Y. Wang, Y. Yu, E. Ma, Z. Hu, J. Phys.: Condens. Matter 17 (2005) 6545.
[6] Y. Kishi, S. Tanabe, S. Tochino, G. Pezzotti, J. Am. Ceram. Soc. 88 (2005) 3423.
[7] L. Huang, T. Yamashita, R. Jose, Y. Arai, T. Suzuki, Y. Ohishi, Appl. Phys. Lett. 90 (2007) 13116.
[8] M.J. Dejneka, J. Non-cryst. Solids 239 (1998) 149.
[9] X. jun Wang, S.H. Huang, R. Reeves, W. Wells, M.J. Dejneka, R.S. Meltzer, W.M. Yen, J. Lumin. 94-95 (2001) 229.
[10] S. Tanabe, H. Hayashi, T. Hanada, N. Onodera, Opt. Mater. 19 (2002) 343.
[11] D. Chen, Y. Wang, Y. Yu, P. Huang, Appl. Phys. Lett. 91 (2007) 051920.
[12] D. Chen, Y. Wang, Y. Yu, F. Liu, P. Huang, Opt. Lett. 32 (2007) 3068.
[13] F. Weng, D. Chen, Y. Wang, Y. Yu, P. Huang, H. Lin, Ceram. Int. 35 (2009) 2619.
[14] Y. Kalisky, The physics and engineering of solid state lasers, Tutorial Texts in Optical Engineering, vol. TT71, SPIE Publications, Washington, 2006. ISBN 978-0819460943 (Chapter 5).
[15] A.A. Kaminskii, Crystalline Lasers : Physical Processes and Operating Schemes, CRC Press, Boca Raton, FL, 1996. ISBN 978-0849337208.
[16] D. Deng, S. Xu, S. Zhao, C. Li, H. Wang, H. Ju, J. Lumin. 129 (2009) 1266.
[17] D. Deng, S. Xu, R. Bao, S. Zhao, B. Wang, H. Wang, H. Ju, J. Phys. D: Appl. Phys. 42 (2009) 105111.
[18] A.L. Patterson, Phys. Rev. 56 (1939) 978.
[19] P. Scherrer, Nachr. Ges. Wiss. Göttingen 26 (1918) 98.
[20] H.E. Kissinger, Anal. Chem. 29 (1957) 1702.
[21] K.-H. Sun, J. Am. Ceram. Soc. 30 (1947) 277.
[22] C.M. Baldwin, D. Mackenzie, J. Am. Ceram. Soc. 62 (1979) 537.
[23] W.J. Miniscalco, in: M.J.F. Digonnet (Ed.), Rare Earth Doped Fiber Lasers and Amplifiers, second ed., Stanford University Press, Stanford, 2001, pp. 17–112.
[24] J.E. Shelbyj, J. Vitko, R.E. Benner, J. Am. Ceram. Soc. 65 (1982) C59.
[25] H. Ebendorff-Heidepriem, W. Seeber, D. Ehrt, J. Non-cryst. Solids 163 (1993) 74.
[26] M.D. O Donnell, C.A. Miller, D. Furniss, V.K. Tikhomirov, A.B. Seddon, J. Non-cryst. Solids 331 (2003) 48.
[27] R. Reisfeld, C.K. Jørgensen, in: A. Gschneider, L. Eyring (Eds.), Handbook on the Physics and Chemistry of Rare-earths, vol. 9, Elsevier, 1987, pp. 1–90. Chapter 58.
[28] J.A. Harrington, Infrared Fibers and Their Applications, SPIE Press, Bellingham, WA, 2004. ISBN 0-8194-5218-1.
[29] W. Koechner, Solid-state laser engineering, in: Optical Sciences, 6th ed., Springer, New York, 2006. ISBN 978-0387290942.
[30] Z. Strnad, Glass–ceramic materials, Glass Science and Technology, Vol. 8, Elsevier, Amsterdam, 1986. ISBN 0-444-99524-2.